Rapid response of New England rivers to shifting boundary conditions: processes, timeframes, and pathways to post-flood channel equilibrium

Carl E. Renshaw[1], Francis J. Magilligan[2], Helen G. Doyle[1], Evan N. Dethier[1], and Keith K. Kantack[1]

[1]*Department of Earth Sciences, Dartmouth College, Hanover, NH 03755*

[2]*Department of Geography, Dartmouth College, Hanover, NH 03755*

ABSTRACT

The timescale of channel recovery from disturbances indicates fluvial resiliency. Quantitative predictions of channel recovery are hampered by multiple possible recovery pathways and stable states and limited long-term observations that provide benchmarks for testing proposed metrics. We take advantage of annual channel change measurements following Tropical Storm Irene's 2011 landfall in New England (USA) to document geomorphic recovery processes and pathways towards equilibrium. A covariate metric demonstrates that channels can adjust rapidly to on-going boundary condition shifts, but that they adjust along a continuum of possible stable states. Moreover, the covariate equilibrium metric indicates sensitivity to warm-season high discharges that, in this region, are increasing in frequency. These data also show that the channels are resilient in that they are able to recover an equilibrium form within 1 to 2 years of disturbances.

INTRODUCTION

The timescale of channel recovery from the acute disturbance of extreme floods provides an important proxy for fluvial resiliency to projected climate-induced changes where the frequency of extreme floods is expected to increase (Tabacchi et al., 2009; Frei et al., 2015; Collins, 2019). Early channel-recovery research presumed that a channel's equilibrium form is uniquely defined such that, given sufficient time, favorable climate, and stable boundary conditions, the channel recovers its pre-disturbance morphology (Schumm and Lichty, 1963; Costa, 1974). Recent work, however, recognizes that multiple possible paths and outcomes characterize channel recovery (Phillips, 2009; Dade et al., 2011; Major et al., 2019). Yet little agreement exists on how to quantify fluvial equilibrium given the multiple possible recovery pathways and stable states. East et al. (2018) observed a shift in sediment flux after a series of moderate flood events and Rathburn et al. (2018) proposed that equilibrium could be identified by the return of sediment flux to pre-disturbance values rather than by channel adjustments. However, since disturbances to sediment source fluxes may recover at rates that are faster than the channel's recovery rate, a return to pre-disturbance sediment flux may not coincide with the establishment of channel geomorphic equilibrium (Rathburn et al., 2018).

Few long-term datasets of coupled response and recovery observations are available to test equilibrium metrics. To address this limitation, we take advantage of Tropical Storm Irene's 2011 landfall in New England. Irene (recurrence interval > 100 years) generated record floods for most of Vermont, western New Hampshire and northern Massachusetts (Fig. 1) with a range of geomorphic impacts (Buraas et al., 2014; Gartner et al., 2015; Magilligan et al., 2015). We build on a pre- and post-Irene database of topographic transects and grain size measurements to better explicate geomorphic recovery processes and pathways towards equilibrium with keen attention to the covariate ways that channel morphologies and bed grain size adjust over time. We show that a covariate metric of channel equilibrium permits situating the recovery process in a broader relation to climate, especially to on-going regional climate shifts.

COVARIATE EQUILIBRIUM METRIC

Quantifying channel equilibrium necessitates coupling channel morphological adjustments to sediment transport (Dade and Friend, 1998; Dade et al., 2011). Our approach is rooted in conventional sediment transport equations that often define sediment flux Q_s as

$$Q_s \propto b\left(\theta - \theta_{cr}\right)^a \qquad \theta \geq \theta_{cr} \ , \tag{1}$$

where the Shields parameter θ is a dimensionless ratio of bed shear stress to submerged particle weight with a critical value θ_{cr} corresponding to the onset of significant sediment motion, and the coefficients a and b are assumed constant for a given sediment transport mode (Dade et al., 2011). Assuming that the dominant sediment transport mode is constant, for a given discharge for which $\theta > \theta_{cr}$, the sediment flux ratio after and before a disturbance Q_{s*} is

$$Q_{s*} \equiv \frac{Q_s^{post}}{Q_s^{pre}} = \left(\frac{\theta^{post} - \theta_{cr}}{\theta^{pre} - \theta_{cr}}\right)^a = \left(\frac{\theta_* - \theta_{cr*}}{1 - \theta_{cr*}}\right)^a \ , \tag{2}$$

where $\theta_* \equiv \theta^{post} / \theta^{pre}$ and $\theta_{cr*} \equiv \theta_{cr} / \theta^{pre}$. This equation can be rearranged as

$$\theta_* = (1 - \theta_{cr*}) Q_{s*}^{1/a} + \theta_{cr*} \ . \tag{3}$$

In bed-load dominated rivers, bankfull discharge has been observed to exhibit just the necessary competence to move sediment, i.e., $\theta_{bankfull} \approx \theta_{cr}$ (Dade and Friend, 1998). This observation assumes the grain size used to define the Shields parameter equals the median grain size (D_{50}) and is limited to systems lacking localized flow complexity due to, for example, large woody debris. With this caveat, assuming the channel is in equilibrium prior to a disturbance, at bankfull discharge $\theta_{cr*} \approx 1$. It follows from Eq. (3) and the assumption that θ_{cr} is a constant that for an equilibrium channel at bankfull discharge (Dade et al., 2011)

$$\theta_* \approx \theta_{cr*} \approx 1. \tag{4}$$

Dade et al. (2011) showed that by expressing θ as a function of a dimensionless friction coefficient (see supplemental material), Eq. (4) can be equivalently expressed as

$$W_* D_*^{3/2} S_*^{-1} \approx Q_* \ , \tag{5}$$

where the subscript (*) indicates dimensionless ratios of bankfull width *W*, bed grain size *D*, slope *S*, and discharge *Q* before and after the disturbance. Assuming the disturbance does not significantly change the bankfull discharge ($Q_* \approx 1$), Eq. (5) shows that, for example, a channel widened during an extreme discharge can return to equilibrium through a corresponding change in S_* and/or D_* even if the width does not return to its pre-disturbance dimension. Thus Eq. (5) explicitly allows for multiple stable channel states. Post-Irene field observations revealed few significant channel course changes, with no avulsions or significant meandering near the transects discussed here (Magilligan et al., 2015). Hence slopes near the transects have been preserved ($S_* \approx 1$), and the covariate equilibrium condition can be simplified as

$$W_* D_*^{3/2} \approx 1 \ . \tag{6}$$

EXAMPLE APPLICATION: SITES AND METHODS

To demonstrate the covariate equilibrium metric, we take advantage of monumented topographic cross-sections impacted by Irene (n = 15, Figure 1 and supplemental material), surveyed before Irene, within three months after, and then once per year until 2017. Because of logistical constraints, not all sites were surveyed yearly. The channels are all gravel-bedded with slopes ranging from 0.001 to 0.027. Transect drainage areas range from 30 to 320 km^2. Large woody debris is generally absent from all transects. At each cross-section, pebble counts (Wolman, 1954) were used to determine D_{50} (Supplemental Table S1). Two-year recurrence annual peak discharges at the transects estimated using StreamStats (Ries et al., 2017) and assumed to approximate bankfull discharges (Andrews, 1980; Emmett and Wolman, 2001), range from 12.5 to 144 m^3s^{-1}. Regional discharge measurements were obtained from five U.S. Geological Survey (USGS) stream gages in the study region (Fig. 1).

Cross sections were used to determine bankfull width and depth. The bankfull stage elevation (using same datum as the transects) was determined in the field prior to Irene. Flow models using the measured changes in channel morphology revealed that channel width and depth changes were generally sufficiently small that the bankfull stage could be assumed approximately constant. Bankfull widths were determined by the intersection of the topographic cross-section and the bankfull stage, and bankfull depth as the quotient of bankfull cross-sectional area and width. In each sampling year, all metrics were normalized by their pre-Irene values, and the normalized values averaged over all transects measured that year to calculate W_* and D_* and their standard errors. Standard significance tests determined the probability p that the average normalized values differed from pre-Irene values.

RESULTS

Channel Width, Depth, and Area

Morphologic responses to Irene floods varied broadly. For example, five sites widened, three narrowed, and width changes at the remaining seven sites were within the measurement uncertainty (~2%). Channel widening was spatially infrequent and limited in magnitude, exceeding 10% at only two sites, likely due to Irene's short duration and stabilizing bank vegetation (Magilligan et al., 2015). Similarly variable channel depth and D_{50} changes occurred. On average, measured channels slightly widened (3%), deepened (6%), and coarsened (4%), but none of these changes are statistically significant ($p > 0.05$; Fig. 2).

Relative to pre-Irene values, no significant channel width or depth changes ($p>0.05$) occurred in the six years after Irene. The greatest change occurred in year two when average channel depth decreased 10% relative to pre-Irene depths, yet even this change was not significant ($p = 0.1$). The only significant change in individual channel properties over the period of record was significant fining of D_{50} in years two ($p < 0.01$) and six ($p = 0.01$). Overall, no consistent pattern emerges in individual metric variation following Irene nor in channel cross-sectional area, which could potentially compensate for variations in the singular channel morphology metrics.

Covariate Equilibrium

To represent covariate changes in channel properties over time, in Figure 3 we plot width change versus grain size change along with the equilibrium condition $W_* D_*^{3/2} = 1$ (Eq. 6). Only in years two ($p < 0.01$) and six ($p = 0.01$) are the covariate changes in the channel properties significantly different from the equilibrium configuration. In both cases the disequilibrium results mostly from channel bed fining. This same plot for transects with complete annual data shows similar patterns.

Bed fining raises the possibility that the dominant mode of sediment transport changed from bedload to mixed load, invalidating the assumption that coefficients a and b are constant.

However, most systems are bed-load dominated when $D_{50} \geq \sim 1$ cm (Dade et al., 2011) and although we observe significant fining at some sites, $D_{50} \geq 1$ cm at all sites.

Figure 3 also indicates that the marginally significant increase in average channel width in year five ($p = 0.09$) is accompanied by a reduction in average grain size – consistent with the predictions of the covariate equilibrium condition (Eq. 6). Accordingly, although the channels widened in year five, they maintained an equilibrium form, demonstrating the multiple stable channel form states. Finally, Figure 3 also shows the rapid channel recovery following deviation from the equilibrium line, such as after Irene and after year two. In both cases, the channel adjusts back toward the equilibrium line in the subsequent years. After the smaller disequilibrium due to Irene, the channels reached equilibrium after one year, while after the larger year two disequilibrium, it required two years.

Discussion

Although Irene locally induced large changes in channel geometry and bed grain size (Buraas et al., 2014; Gartner et al., 2015; Magilligan et al., 2015), and initiated or reactivated nearly one thousand channel-proximal landslides (Dethier et al., 2016), when the geomorphic changes in normalized channel width, depth, cross-sectional area, and D_{50} are averaged over the impacted region (Fig. 1), little net changed occurred. That is, average channel incision, widening, and coarsening were nearly balanced by average channel aggradation, narrowing, and fining, respectively (Gartner et al., 2015).

The limited impact of Irene flooding on average channel morphology makes the significant disequilibrium apparent in years two and six (Fig. 3) surprising given the modest peak discharges in post-Irene years. Average peak Irene discharge was nearly five times the 2-year recurrence interval instantaneous peak discharge Q_2 (Fig. 1 inset). Since Irene, the ratio of annual instantaneous peak discharges Q_{peak} to Q_2 exceeded two only once at one site.

To further explore the linkage between hydrologic shifts and channel disequilibrium, we analyzed the timing and magnitude of the five highest daily mean discharges Q_{daily} for each year on each gaged river (Fig. 4). To compare across watersheds, Q_{daily} was normalized by Q_2. Relatively high discharges ($Q_{daily}/Q_2 > \sim 0.5$) occurred not only in the two years with significant disequilibrium, years two (2013) and six (2017), but also in years three (2014) and five (2016). However, the high discharge timing in the equilibrium years (three and five) differs from the disequilibrium years (two and six); significant disequilibrium occurred only when high discharges occurred in summer months (shaded regions in Fig. 4). That is, both the magnitude and timing of high discharges regulate their impact on the channel, with warm season events impacting the channel more than cold season ones. This is noteworthy in that warm season high discharges have become more frequent in New England since 1996 (Frei et al., 2015; Collins, 2019). That is, the more frequent high discharge types (i.e., warm season high discharges) are those that generate the greatest impact on channel properties, most notably channel bed fining. Channel bed finding is widely recognized to negatively impact aquatic ecosystems (Kemp et al., 2011). The consistency of the fining across multiple, dispersed sites argues against a localized sediment source due to, for example, logging, plowing, or road construction. Instead, fining likely occurs because of finer sediment delivered from new and reactivated landslides that occurred during Irene. (Grain size distributions and a photo of typical landslide are given in supplemental material.) Dethier et al. (2016) showed that landslide scars continue to provide elevated sediment inputs years after Irene. Because the landslides are frozen or snow-covered in the winter and early spring, cold season high discharges are less effective at mobilizing sediment from these landslides. In total, these results suggest that regional climate shifts currently underway (Frei et al., 2015; Collins, 2019) are beginning to manifest geomorphologically.

Although the covariate equilibrium metric record indicates enhanced sensitivity to warm season high discharges, the same record also shows that the channels are resilient in that they recover to an equilibrium form within 1 to 2 years after major geomorphic events. The rapid channel recovery is supported by the region's humid climate (Wolman and Gerson, 1978) and abundant supply of sediment (Brierley et al., 2005) from glacial deposits. However, the recovered channel forms differ from pre-Irene forms; they are, on average, slightly wider, deeper, and finer. This shift in equilibrium form highlights the advantage of the covariate equilibrium metric. For example, in year five the channels were, on average, 9% wider than pre-Irene, a marginally significant change (p = 0.09). Considering width alone, we might conclude that the channels had not recovered. However, that same year the covariate equilibrium parameter $W_*D_*^{3/2}$ only differs from its pre-Irene value by 2%, a non-significant change (p = 0.44). In fact, the covariate equilibrium parameter indicates that by year five, channels had recovered an equilibrium form twice, first from the marginally significant disequilibrium induced by Irene and then from the disequilibrium induced by the year 2 warm season high discharges. The covariate metric demonstrates that channels can adjust rapidly to on-going boundary condition shifts, but that they adjust along a continuum of possible stable states. With the manifold complexity of geomorphic systems, it may never be possible to specifically predict geomorphic recovery's timing and pathways, but these results provide a template to capture channel evolution following a disturbance.

ACKNOWLEDGMENTS

This research was supported in part by the National Science Foundation (BCS-1636415). We thank Jon Major, Sara Rathburn, and an anonymous reviewer for their thoughtful comments and suggestions that greatly improved the manuscript.

REFERENCES CITED

Andrews, E. D., 1980, Effective and Bankfull Discharges of Streams in the Yampa River Basin, Colorado and Wyoming: Journal of Hydrology, v. 46, no. 3-4, p. 311-330.

Brierley, G. J., Brooks, A. P., Fryirs, K., and Taylor, M. P., 2005, Did humid-temperate rivers in the Old and New Worlds respond differently to clearance of riparian vegetation and removal of woody debris?: Progress in Physical Geography, v. 29, no. 1, p. 27-49.

Buraas, E. M., Renshaw, C. E., Magilligan, F. J., and Dade, W. B., 2014, Impact of reach geometry on stream channel sensitivity to extreme floods: Earth Surface Processes and Landforms, v. 39, no. 13, p. 1778-1789.

Collins, M. J., 2019, River flood seasonality in the Northeast United States: Characterization and trends: Hydrological Processes, v. 33, p. 687-698.

Costa, J. E., 1974, Response and recovery of a piedmont watershed from tropical storm Agnes, June 1972: Water Resources Research, v. 10, no. 1, p. 106-112.

Dade, W. B., and Friend, P. F., 1998, Grain size, sediment-transport regime and channel slope in alluvial rivers: J. Geol., v. 106, p. 661-675.

Dade, W. B., Renshaw, C. E., and Magilligan, F. J., 2011, Sediment transport constraints on river response to regulation: Geomorphology, v. 126, no. 1-2, p. 245-251.

Dethier, E., Magilligan, F. J., Renshaw, C. E., and Nislow, K. H., 2016, The role of chronic and episodic disturbances on channel-hillslope coupling: the persistence and legacy of extreme floods: Earth Surface Processes and Landforms, v. 41, no. 10, p. 1437-1447.

East, A. E., Stevens, A. W., Ritchie, A. C., Barnard, P. L., Campbell-Swarzenski, P., Collins, B. D., and Conaway, C. H., 2018, A regime shift in sediment export from a coastal watershed during a record wet winter, California: Implications for landscape response to hydroclimatic extremes: Earth Surface Processes and Landforms, v. 43, no. 12, p. 2562-2577.

Emmett, W. W., and Wolman, M. G., 2001, Effective discharge and gravel-bed rivers: Earth Surface Processes and Landforms, v. 26, no. 13, p. 1369-1380.

Frei, A., Kunkel, K. E., and Matonse, A., 2015, The seasonal nature of extreme hydrological events in the Northeastern United States: Journal of Hydrometeorology, v. 16, no. 5, p. 2065-2085.

Gartner, J. D., Magilligan, F. J., and Renshaw, C. E., 2015, Predicting the type, location and magnitude of geomorphic responses to dam removal: Role of hydrologic and geomorphic constraints: Geomorphology, v. 251, p. 20-30.

Kemp, P., Sear, D., Collins, A., Naden, P., and Jones, I., 2011, The impacts of fine sediment on riverine fish: Hydrological Processes, v. 25, no. 11, p. 1800-1821.

Magilligan, F. J., Buraas, E. M., and Renshaw, C. E., 2015, The efficacy of stream power and flow duration on geomorphic responses to catastrophic flooding: Geomorphology, v. 228, p. 175-188.

Major, J. J., Zheng, S., Mosbrucker, A. R., Spicer, K. R., Christianson, T., and Thorne, C. R., 2019, Multidecadal geomorphic evolution of a profoundly disturbed gravel bed river system—A complex, nonlinear response and Its Impact on sediment delivery: Journal of Geophysical Research, v. 124, p. 1281–1309.

Phillips, J. D., 2009, Changes, perturbations, and responses in geomorphic systems: Progress in Physical Geography, v. 33, no. 1, p. 17-30.

Rathburn, S. L., Shahverdian, S. M., and Ryan, S. E., 2018, Post-disturbance sediment recovery: Implications for watershed resilience: Geomorphology, v. 305, p. 61-75.

Ries, K. G., III, J.K., N., Smith, M. J., Guthrie, J. D., Steeves, P. A., Haluska, T. L., Kolb, K. R., Thompson, R. F., Santoro, R. D., and Vraga, H. W., 2017, StreamStats, version 4: U.S. Geological Survey Fact Sheet, v. 2017–3046.

Schumm, S. A., and Lichty, R. W., 1963, Channel widening and floodplain construction along Cimarron River in Southern Kansas: U.S. Geological Survey Professional Paper, v. 352-D, p. 71-88.

Tabacchi, E., Steiger, J., Corenblit, D., Monaghan, M. T., and Planty-Tabacchi, A. M., 2009, Implications of biological and physical diversity for resilience and resistance patterns within Highly Dynamic River Systems: Aquatic Sciences, v. 71, no. 3, p. 279-289.

USGS, 1982, Guidelines for determining flood flow frequency, Reston, Virginia, United States Geological Survey.

Wohl, E. E., Anthony, D. J., Madsen, S. W., and Thompson, D. M., 1996, A comparison of surface sampling methods for coarse fluvial sediments: Water Resources Research, v. 32, no. 10, p. 3219-3226.

Wolman, M. G., 1954, A method of sampling coarse river-bed material: Trans Amer Geophy Union, v. 35, no. 6, p. 951-956.

Wolman, M. G., and Gerson, R., 1978, Relative scales of time and effectiveness of climate in watershed geomorphology: Earth Surface Processes and Landforms, v. 3, no. 2, p. 189-208.

FIGURE CAPTIONS

Figure 1. Locations of measured transects and USGS gaging stations. Transect names in italics. Photos of all site are available in the supplemental material. At most sites paired (upstream and downstream) transects were measured. Inset shows magnitude and timing of annual (water year) peak instantaneous discharge at each gage between the years 2011-2017. For clarity, timing of 2014 peaks for AB and DR are offset by plus and minus one month, respectively. Peak discharges are normalized by the 2-year recurrence interval discharge as determined from log Pearson analysis of annual peak instantaneous discharges recorded at each gage. Gage names (USGS number): AB = Ayers Brook (01142500), MR = Mad River (04288000), DR = Dog River (04287000), PR = Pemigewasset River (01076500), WR = Walloomsac River (01334000).

Figure 2. Average changes in bankfull cross-sectional width, depth, and median grain size (D_{50}) since Tropical Storm Irene. Following Wohl et al. (1996), uncertainty associated with grain measurements was assumed to be ± 12%. Error bars indicate ± one standard error. Times for the depth and grain size are offset by ± 0.1 year to increase legibility. Topographic transects are given in the supplemental material.

Figure 3. Changes in average normalized width W_* plotted against changes in median grain size D_* over time. Here "Pre" refers to the survey completed before Irene and "Post" refers to the survey completed within three months after Irene. Values of averaged over all transects. Dashed line indicates states of equilibrium as defined by Eqn. (6). Error bars represent one standard error.

Figure 4. Five highest daily mean discharges on each gaged river for each year since Irene. Discharges are normalized by the two-year instantaneous peak discharge as determined from a log-Pearson analysis of annual peak discharges recorded at each gage (USGS, 1982). Shaded regions indicate summer season for each year.

[1]GSA Data Repository item 201Xxxx, Table of measured bankfull widths, depths, and grain sizes, photographs and topographic cross-sections of each transect, aggregate grain size distributions, and photograph of typical channel-adjacent landslide, is available online at www.geosociety.org/pubs/ft20XX.htm, or on request from editing@geosociety.org or Documents Secretary, GSA, P.O. Box 9140, Boulder, CO 80301, USA.

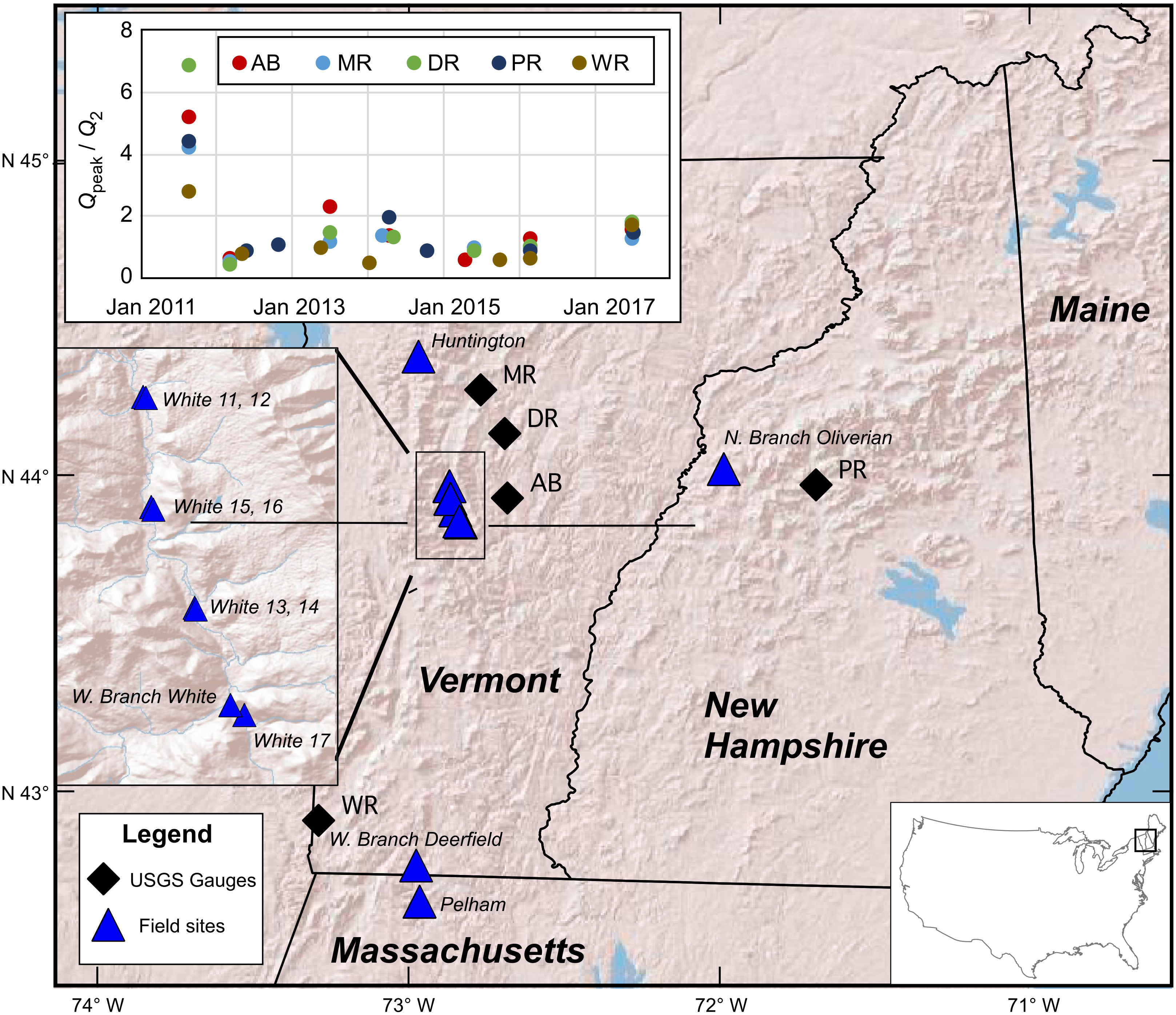

Figure 1. Locations of measured transects and USGS gaging stations. Transect names in italics. Photos of all site are available in the supplemental material. At most sites paired (upstream and downstream) transects were measured. Inset graph shows magnitude and timing of annual instantaneous peak discharge at each gage between the years 2011-2017. For clarity, timing of 2014 peaks for AB and DR are offset by plus and minus one month, respectively. Peak discharges are normalized by the 2-year recurrence interval discharge as determined from log Pearson analysis of annual peak instantaneous discharges recorded at each gage. Gage names (USGS number): AB = Ayers Brook (01142500), MR = Mad River (04288000), DR = Dog River (04287000), PR = Pemigewasset River (01076500), WR = Walloomsac River (01334000).

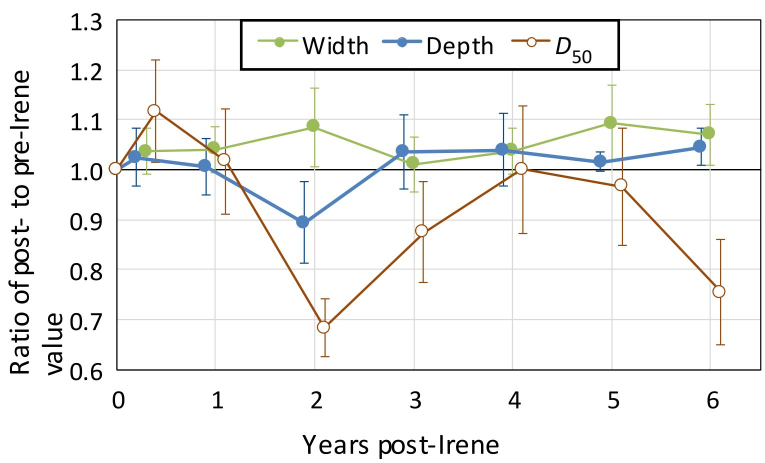

Figure 2. Average changes in bankfull cross-sectional width, depth, and median grain size (D_{50}) since Tropical Storm Irene. Following Wohl et al. [, 1996 #2066], uncertainty associated with grain measurements was assumed to be ± 12%. Error bars indicate ± one standard error. Times for the depth and grain size are offset by ± 0.1 year to increase legibility.

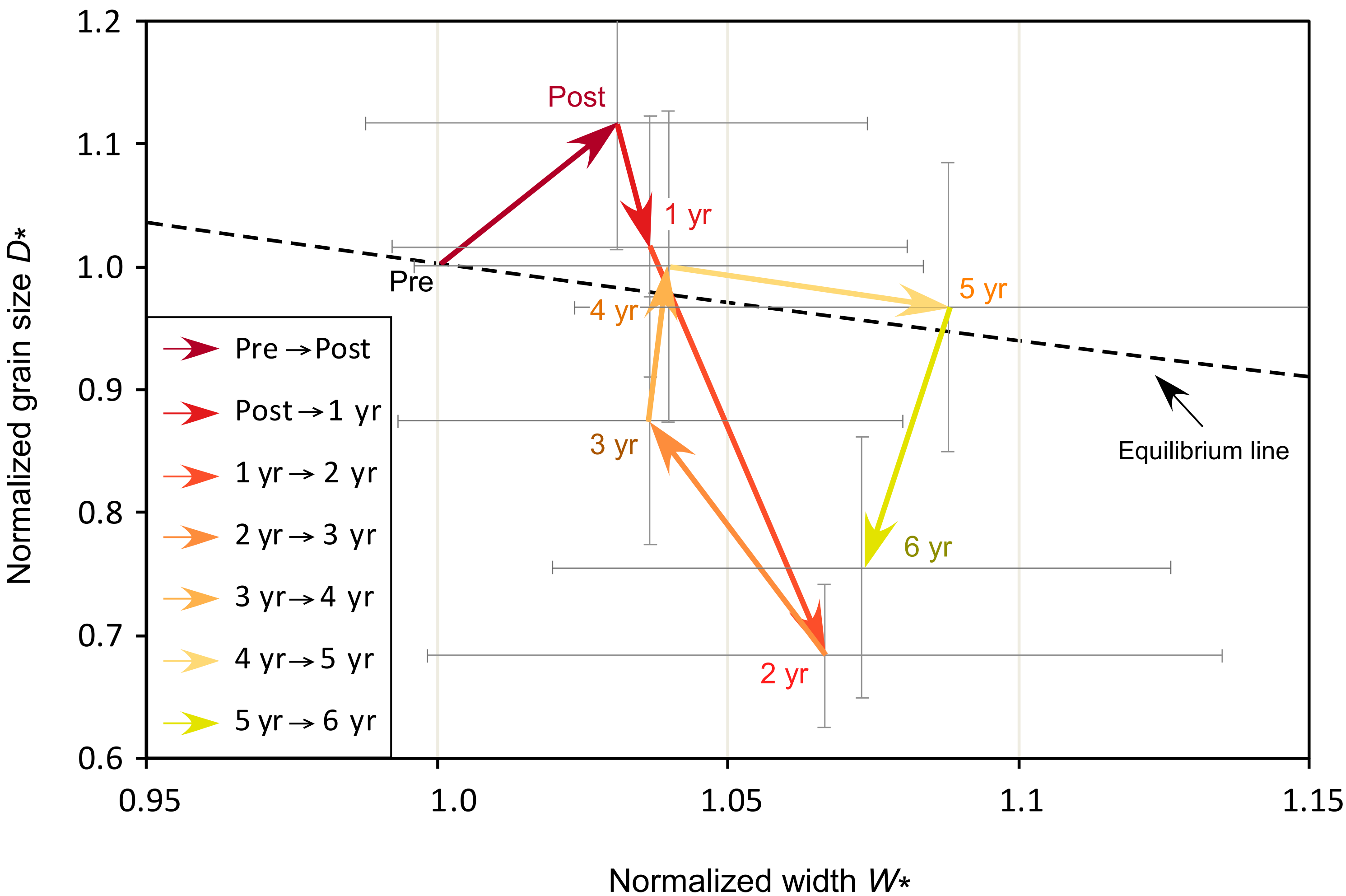

Figure 3. Changes in average width and median grain size over time normalized by their pre-Irene values. Here "Pre" refers to the survey completed before Tropical Storm Irene and "Post" refers to the survey completed within three months after Irene. Values are averaged over all transects. Dashed line indicates states of equilibrium as defined by Equation 6 in text. Error bars represent one standard error.

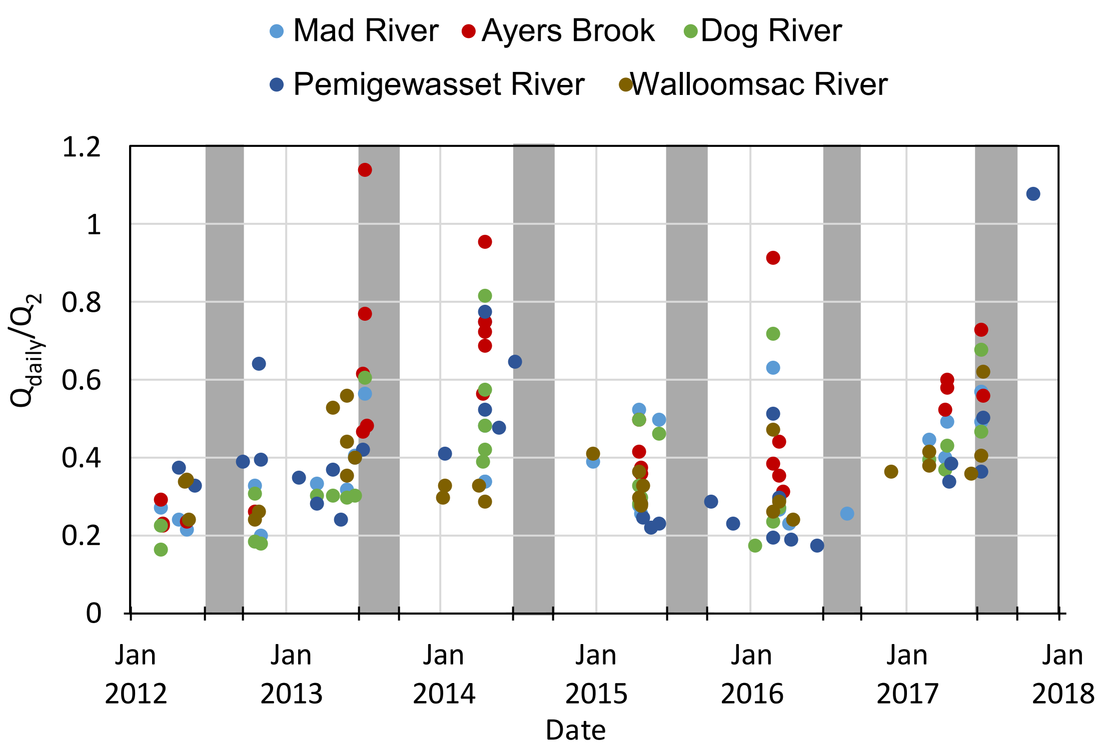

Figure 4. Five highest daily mean discharge Q_{daily} on each gaged river for each year since Irene. Discharges are normalized by the two-year instantaneous peak discharge Q_2 as determined from a log-Pearson analysis of annual peak discharged recorded at each gage (England et al., 2019). Shaded regions indicate summer season for each year.